

TEMPORALLY TRANSFERABLE MACHINE LEARNING MODEL FOR TOTAL SUSPENDED MATTER RETRIEVAL FROM SENTINEL-2

Milad Niroumand-Jadidi ^{1,*}, Francesca Bovolo ¹

¹ Digital Society Center, Fondazione Bruno Kessler, Via Sommarive, 18 I-38123, Trento, Italy; (mniroumand, bovolo)@fbk.eu

Commission III, WG III/9

KEY WORDS: total suspended matter, water quality, Sentinel-2, machine learning, band ratio, model transferability, sun glint

ABSTRACT:

The empirical (regression-based) models have long been used for retrieving water quality parameters from optical imagery by training a model between image spectra and collocated in-situ data. However, a need clearly exists to examine and enhance the temporal transferability of models. The performance of a model trained in a specific period can deteriorate when applied at another time due to variations in the composition of constituents, atmospheric conditions, and sun glint. In this study, we propose a machine learning approach that trains a neural network using samples distributed in space and time, enabling the temporal robustness of the model. We explore the temporal transferability of the proposed neural network and standard band ratio models in retrieving total suspended matter (TSM) from Sentinel-2 imagery in San Francisco Bay. Multitemporal Sentinel-2 imagery and in-situ data are used to train the models. The transferability of models is then examined by estimating the TSM for imagery acquired after the training period. In addition, we assess the robustness of the models concerning the sun glint correction. The results imply that the neural network-based model is temporally transferable ($R^2 \approx 0.75$; $RMSE \approx 7 \text{ g/m}^3$ for retrievals up to 70 g/m^3) and is minimally impacted by the sun glint correction. Conversely, the ratio model showed relatively poor temporal robustness with high sensitivity to the glint correction.

1. INTRODUCTION

Earth observation has spurred significant advances in monitoring the quality of inland and coastal waters (Sagan et al., 2020). The undeniable role of remote sensing is mainly due to providing spatiotemporally explicit information on the status of in-water constituents contrary to field-based measurements limited in both space and time (Hansen et al., 2017; Ritchie et al., 2003). Remotely mapping constituents like chlorophyll-a (Chl-a) has a sound background in open oceans known as case-I waters (Groom et al., 2019; Vandermeulen et al., 2020). However, inland and nearshore waters (case-II) represent different bio-optical conditions than oceanic ones. They are optically more complex as phytoplankton communities do not dominate the bio-optical condition. So, other constituents like total suspended matter (TSM) and colored dissolved organic matter (CDOM) can also vary largely in inland and nearshore coastal waters, posing more complexities and spectral ambiguities (Defoin-Platel and Chami, 2007; Niroumand-Jadidi et al., 2021). There might also be confounding effects from the bottom-reflected radiance in shallow and clear waters (Niroumand-Jadidi et al., 2020a), further complicating constituent retrieval. On the other hand, the spatial resolution of the common ocean color sensors (e.g., Sentinel-3) is too coarse to capture most of the inland waters like lakes and rivers. With the launch of Operational Land Imager (OLI) and Multispectral Instrument (MSI) sensors, onboard Landsat-8 and Sentinel-2 satellites, retrieval of constituents in inland and nearshore coastal waters received increasing interest (Niroumand-Jadidi et al., 2019; Toming et al., 2016). These satellite sensors provide sufficient spatial resolution (10–30 m) and a radiometric resolution (12 bit) sensitive to the changes in the water-leaving radiance (Toming et al., 2016). Having a high radiometric resolution is of particular importance due to the low signal-to-noise ratio (< 15%) of water bodies (Jorge et al., 2017). Moreover, although OLI and MSI are not designed specifically for aquatic applications, the spectral resolutions of the sensors are suitable for accurate retrieval of water quality parameters (Bresciani et al., 2020; Niroumand-Jadidi et al., 2021).

There are various methods developed to estimate water quality indicators from optical imagery that fall into three main approaches: (i) empirical (regression-based) models that establish a relation between image-derived spectral features and associated water quality parameters measured in the field (Gholizadeh et al., 2016; Niroumand-Jadidi et al., 2019); (ii) physics-based models that rely on a radiative transfer model to invert image spectra to inherent optical properties (IOPs) and concentration of constituents (Gege, 2004; Mobley, 1994; Niroumand-Jadidi et al., 2020c); (iii) semianalytical (quasi-analytical) algorithms that are a blend of empirical relationships and radiative transfer theory (Lee et al., 2002; Pitarch and Vanhellemont, 2021). Although each modeling approach has pros and cons, empirical methods remain the most popular among others (Gholizadeh et al., 2016; Niroumand-Jadidi et al., 2019; Toming et al., 2016). The empirical methods are relatively straightforward and fast to apply with minimal need to adhere to the underlying physics (Niroumand-Jadidi et al., 2018). Moreover, when trained and applied on the same image, the regression-based models (e.g., band ratios) are proven to have less sensitivity to the quality of atmospheric correction. Even top-of-atmosphere (TOA) data are employed successfully in some studies (Toming et al., 2016). In contrary, physics-based and semianalytical methods are largely impacted by the quality of remote sensing reflectance (R_{rs}) derived after atmospheric correction (Bernardo et al., 2017; Niroumand-Jadidi et al., 2020b).

Despite the widespread use of empirical methods in retrieving water quality parameters, the models' transferability in space and time remains a challenge (Ligi et al., 2017; Politi et al., 2015). The spatiotemporal variations of bio-optical conditions, atmospheric effects, and surface sun glint can degrade the robustness and reliability of regression-based models. This study focuses on TSM retrieval from Sentinel-2 imagery and pursues two main objectives: (i) propose a machine learning-based (neural network) model for an improved temporal transferability compared to standard ratio models. The neural network-based model incorporates visible and near-infrared (VNIR) bands and

* Corresponding author

trains based on samples distributed in space and time to enhance the temporal robustness; (ii) assess the impact of sun glint correction on the robustness of machine learning and ratio models. Sun glint is a confounding factor due to the specular reflection from the water surface that makes the spectra appear brighter than actual and varies spatiotemporally.

The rest of the manuscript is structured as follows: Section 2 describes the proposed machine learning model for TSM retrieval. The case study and the dataset are introduced in Section 3. Section 4 presents the results of experiments and discussion. Finally, the paper concludes in Section 5 by summarizing the key findings and providing a perspective for future studies.

2. METHODS

The temporal transferability of empirical models can be hindered by variation in the range and composition of in-water constituents as well as atmospheric and surface sun glint effects. To overcome this issue, we propose a method based on neural networks leveraging training samples distributed in space and time. The aim of this spatiotemporal learning approach is to enhance the robustness of the model concerning the mentioned confounding factors when transferring the model to a time other than the training period.

First, we apply an atmospheric correction to the multitemporal Sentinel-2 images to mitigate the differences in atmospheric effects. A dark spectrum fitting (DSF) method available in ACOLITE, developed specifically for aquatic applications, is employed for atmospheric correction (Vanhellemont, 2019). We obtain Sentinel-2 R_{rs} images at 10 m spatial resolution from the DSF correction. The atmospherically corrected data are at 11 spectral bands, including nine visible near-infrared (VNIR) and two shortwave infrared (SWIR) bands. The central wavelengths of the DSF-corrected bands are listed for Sentinel-2A in Table 1. The same holds for the Sentinel-2B with slight differences in central wavelengths of some bands. The VNIR bands are considered for TSM retrieval, whereas SWIR bands are used only for the sun glint correction.

Bands	Central wavelengths [nm]
VNIR	443, 492, 560, 665, 704, 740, 783, 833, 865
SWIR	1614, 2202

Table 1. The central wavelengths of Sentinel-2A bands in VNIR and SWIR portions of the spectrum as outputs of the DSF atmospheric correction.

The average R_{rs} spectra are extracted considering 3×3 windows at the location of in-situ data. Then, we split the samples (in-situ TSM coupled with R_{rs}) into training and validation. The validation samples are not seen through the validation but are also temporally independent. In this context, the training is performed with spatiotemporal samples over a given period. Then, the validation is conducted for acquisitions after the training period. This validation scheme allows examining the temporal transferability of the proposed method.

We train a neural network considering VNIR R_{rs} spectra (nine Sentinel-2 bands) as input features and the in-situ TSM values as the target parameter. The proposed neural network architecture involves two hidden layers with 15 neurons in each layer (Figure 1). The number of hidden layers and neurons is defined in an optimization procedure by testing the model's performance by varying the parameters. We hypothesize that training based on the samples with spatiotemporal distribution can improve the robustness of the model due to: (i) increased number of samples when the samples are distributed in both space and time, and (ii) enhanced representativeness of the training data in terms of

capturing the confounding effects (e.g., sun glint, atmospheric effects).

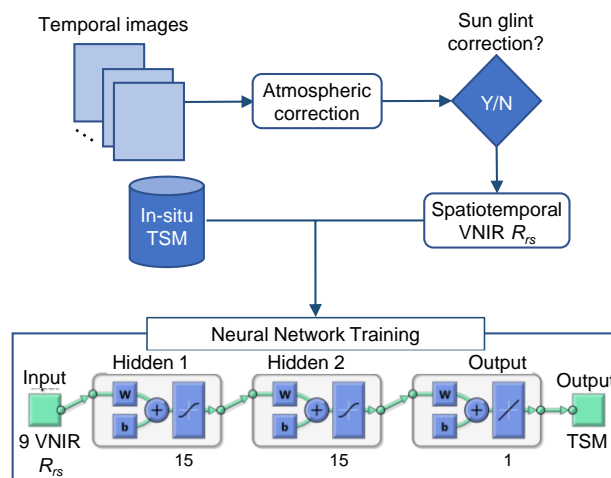


Figure 1. A thematic representation of the proposed machine learning approach for retrieving TSM.

We also train a ratio model, as a standard method, with the same training set considered for the neural network. Although ratio models are widely applied on Sentinel-2 images (Soomets et al., 2020; Toming et al., 2016), the optimal pair of ratio bands to retrieve a given constituent can be variable according to the in-water bio-optical conditions. Therefore, we perform optimal band ratio analysis (OBRA) to identify the bands automatically. OBRA examines all the possible band ratios to identify the one providing the strongest determination coefficient (R^2) for the training data (Legleiter et al., 2009; Niroumand-Jadidi et al., 2019; Niroumand-Jadidi and Vitti, 2016). Different forms of ratio models (e.g., linear and second-order polynomials) can be applied. In this study, an exponential model is chosen as it performed better than other forms:

$$X = \ln \left[\frac{R_{rs}(\lambda_1)}{R_{rs}(\lambda_2)} \right], TSM = ae^{bX}, \quad (1)$$

where $X = \log$ -transformed band ratio feature
 $R_{rs}(\lambda_1) = R_{rs}$ of numerator band
 $R_{rs}(\lambda_2) = R_{rs}$ of denominator band
 $a, b = \text{constant coefficients}$

Besides atmospheric effects, sun glint (i.e., the specular reflection of light from water surfaces) is another confounding factor that can vary spatiotemporally. It can introduce additional noise in retrieving constituents, particularly in a multitemporal context. To investigate the impact of sun glint correction, we train the models (either neural network or band ratio) with spectra corrected for sun glint and once without such correction. We consider a simple sun glint correction by subtracting a SWIR band from all the other bands. This correction is based on the negligible water-leaving radiance over SWIR bands, even for turbid waters. Thus, the signal observed in the SWIR bands is associated with the sun glint effect (Overstreet and Legleiter, 2017; Vanhellemont and Ruddick, 2015). We consider the SWIR band of Sentinel-2 centered at around 2200 nm for the glint correction:

$$R_{rs}^{corrected}(\lambda) = R_{rs}(\lambda) - R_{rs}(SWIR), \quad (2)$$

where $R_{rs}^{corrected}(\lambda) = \text{Sun glint corrected } R_{rs} \text{ at } \lambda$
 $R_{rs}(\lambda) = R_{rs} \text{ at } \lambda$
 $R_{rs}(SWIR) = R_{rs} \text{ at } \sim 2200 \text{ nm}$

The temporal transferability of both ratio and neural network-based models with and without the sun glint correction is examined by performing a matchup analysis between the predicted and measured TSM values for validation samples. We consider a set of metrics for validation, including R^2 , root mean square error (RMSE), bias, and mean absolute error (Seegers et al., 2018):

$$R^2 = \frac{\sum_{i=1}^n (E_i - \bar{M})^2}{\sum_{i=1}^n (O_i - \bar{M})^2}, \quad \bar{M} = \frac{1}{n} \sum_{i=1}^n M_i \quad (3)$$

$$RMSE = \left(\frac{\sum_{i=1}^n (E_i - M_i)^2}{n} \right)^{1/2} \quad (4)$$

$$bias = 10^{\frac{\sum_{i=1}^n \log_{10}(E_i/M_i)}{n}} \quad (5)$$

$$MAE = 10^{\frac{\sum_{i=1}^n |\log_{10}(E_i/M_i)|}{n}} \quad (6)$$

where $n = \text{number of validation samples}$
 $E_i = \text{estimated TSM for the } i\text{th sample}$
 $M_i = \text{measured TSM for the } i\text{th sample}$

3. CASE STUDY AND DATASET

San Francisco Bay is selected as our case study as it represents a relatively wide range of TSM variations spatiotemporally. The in-situ data used in this study are acquired at 30 fixed sampling locations along a transect longer than 100 km. Figure 2 shows the study area captured by Sentinel-2 images (atmospherically corrected by the DSF) on 16 December 2019, along with the location of field stations. The sediment plumes are evident on the upper and lower parts of the bay. The water samples are collected at near-surface ($\sim 1 \text{ m}$ depth) and analyzed in the laboratory to derive the TSM concentration (Cloern et al., 2020; Schraga and Cloern, 2017).

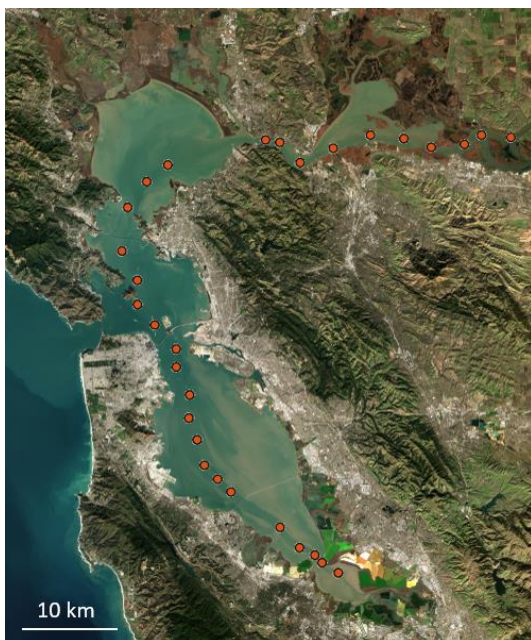
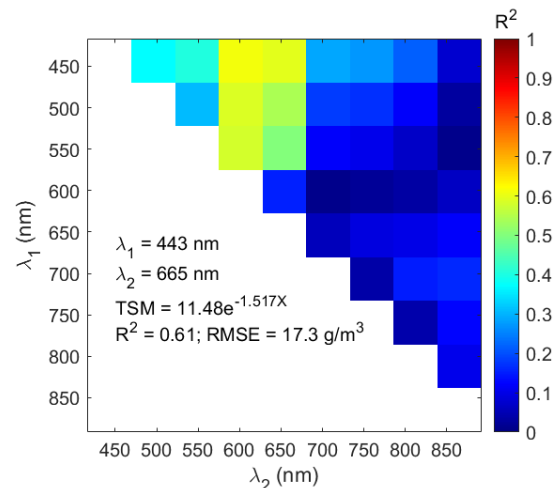


Figure 2. Sentinel-2 images (2019/12/16) over San Francisco Bay processed by ACOLITE atmospheric correction. In-situ measurement stations are shown in red circles.

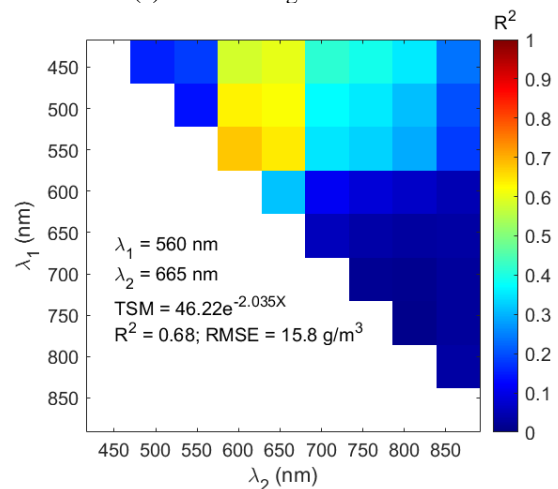
Twelve in-situ acquisition dates spanned over different seasons of 2019 were identified with close (≤ 3 days) Sentinel-2 overpasses. Two Sentinel-2 tiles were required to cover the study area at a given time (thus, 24 images were processed in total). 262 spatiotemporal samples were extracted after atmospheric correction and excluding the samples affected by cloud or haze. The samples associated with the latest three images (70 samples) were reserved for validation to assess the temporal transferability of the models. The TSM concentration of in-situ samples varies from $\sim 2 \text{ g/m}^3$ to $\sim 120 \text{ g/m}^3$, with an average of $\sim 25 \text{ g/m}^3$.

4. RESULTS AND DISCUSSION

The OBRA of training data with and without the sun glint correction is illustrated in Figure 3. The R^2 for all the possible band ratios is shown as a colored matrix. The optimal numerator band changes from a blue band (443 nm) for the case without glint correction (Figure 3a) to a green band (560 nm) for the glint-corrected OBRA (Figure 3b). However, the denominator band remains the same (665 nm). The change in the optimal pair of bands indicates the sensitivity of OBRA to the glint correction to be taken into account when transferring the model temporally. The sun glint correction led to training improvements in R^2 and RMSE on the order of 0.07 and 1.5 g/m^3 , respectively. Figure 4 shows the fit curves and associated exponential models for both cases, i.e., with and without the glint correction.



(a) without sun glint correction



(b) with sun glint correction

Figure 3. Optimal band ratio analysis (OBRA) of training data (a) without and (b) with sun glint correction.

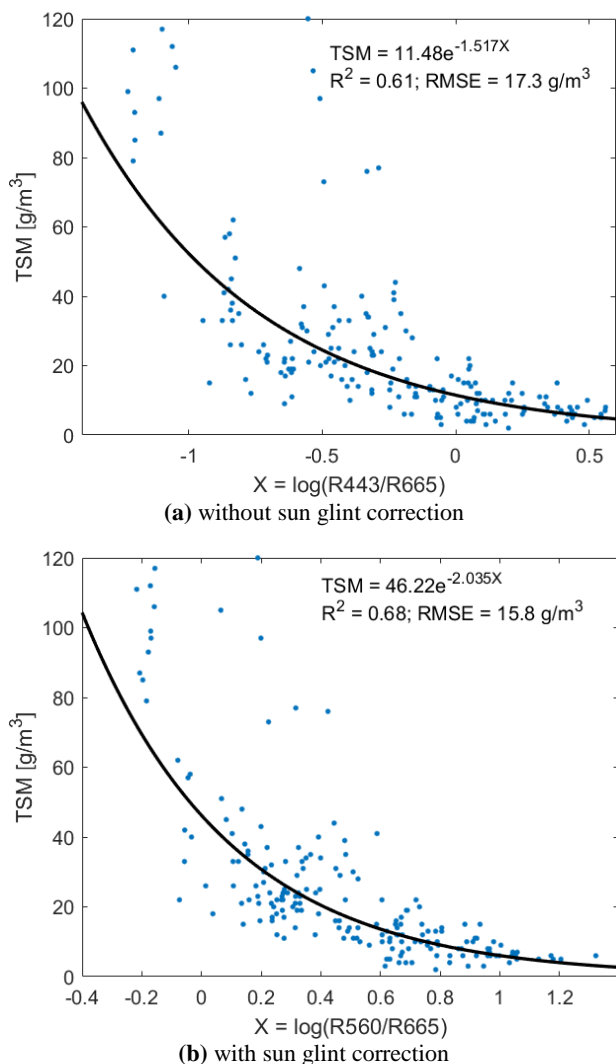


Figure 4. Exponential models for TSM estimation derived from OBRA (a) without and (b) with sun glint correction.

The trained OBRA models (Figure 4) have major differences in terms of the constant parameters a and b for the cases with and without the glint correction. Thus, validation using independent samples can give insights into the reliability and robustness of the models.

Figure 5 shows the in-situ vs. image-derived TSM matchups based on OBRA for the validation samples. The performance of the ratio model is poor without sun glint correction ($R^2 = 0.33$; $RMSE = 12.3 \text{ g/m}^3$). The retrievals improve significantly using the glint corrected model. This finding indicates the sensitivity of OBRA to sun glint variations. Thus, the transferability of OBRA to a time other than the training period requires very accurate R_{rs} data corrected for any temporally induced noise.

The validation matchups are illustrated in Figure 6 for the proposed neural network-based TSM retrieval with and without performing the glint correction. The results convey that accurate TSM retrieval ($R^2 \approx 0.75$; $RMSE \approx 7 \text{ g/m}^3$) is achieved when applying the trained network to images acquired after the training period. The retrievals are minimally affected by the sun glint correction indicating the robustness of the machine learning approach. The neural network-based model takes advantage of all the spectral information (9 R_{rs} bands), unlike OBRA that relies only on a single band ratio. Furthermore, the neural networks are proven to be capable of learning informative and robust features

from the original data without a need for prior extraction of the features. The outperformance of the neural network model compared to the OBRA can be attributed to these characteristics. The extensive accuracy metrics for validation samples are reported in Table 2 for both neural network and OBRA models. The bias of the neural network-based model, either with or without the glint correction, is minimal as it is close to one. On the other hand, the OBRA-based retrievals resulted in a bias significantly smaller than one, indicating underestimated TSM, particularly for the model without glint correction (bias = 0.71; i.e., the estimated TSM is on average ~30% smaller than the actual values). The glint correction improves the results for both neural network and OBRA models. However, the improvements are more pronounced for the OBRA. In the case of OBRA, the glint correction yielded an improvement in R^2 and RMSE of 0.36 and 4.23 g/m^3 , respectively. The MAE of OBRA also improves about 20% by applying the glint correction. However, the neural network-based model provided the most accurate retrieval with an R^2 of 0.76 and an RMSE of 6.3 g/m^3 when the glint correction is applied. The machine learning results without glint correction are also comparable to those derived with the correction.

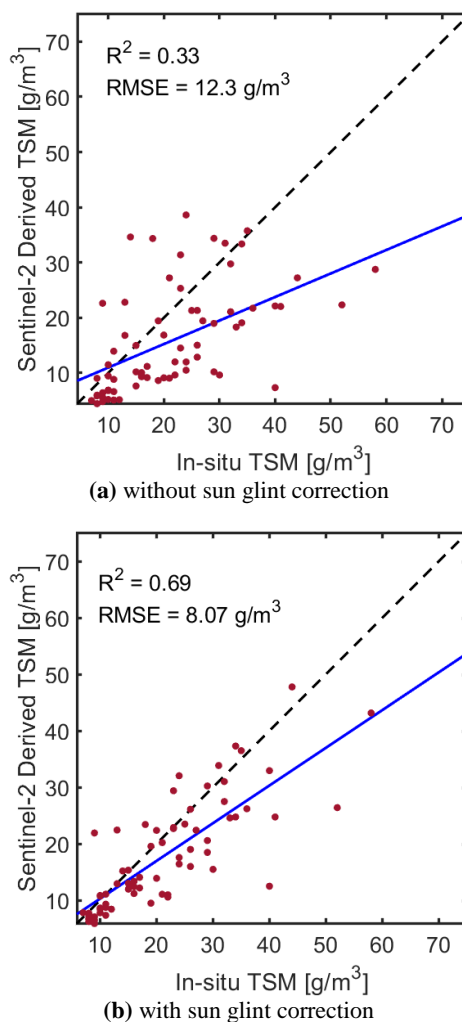


Figure 5. Matchup validation of OBRA-based TSM retrieval to assess the temporal transferability of the model (a) without and (b) with sun glint correction.

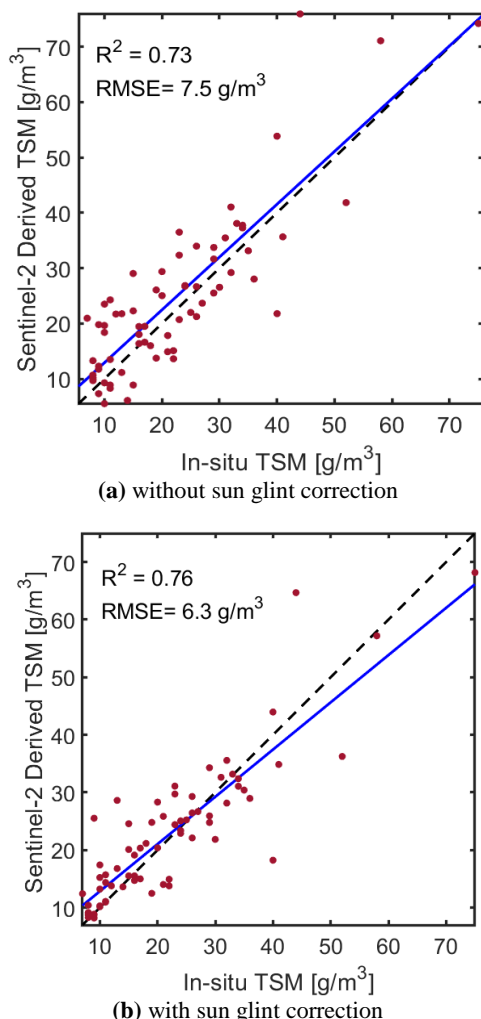


Figure 6. Matchup validation of neural network-based TSM retrieval to assess the temporal transferability of the model (a) without and (b) with sun glint correction.

	Neural Network		OBRA	
	Without GC	With GC	Without GC	With GC
R ²	0.73	0.76	0.33	0.69
RMSE [g/m ³]	7.5	6.3	12.3	8.07
Bias	1.1	1.06	0.71	0.83
MAE	1.34	1.22	1.63	1.31

Table 2. Accuracy statistics of TSM retrieval based on neural network and OBRA models without and with the glint correction (GC).

We apply the trained models on entire image pixels to produce the TSM map. The TSM maps based on OBRA with and without the glint correction are shown in Figure 7 for the image acquired on 16 December 2019 (after the training period). As evident, the sediment plumes, particularly in the lower part of the bay, are mapped more effectively with the glint-corrected model.

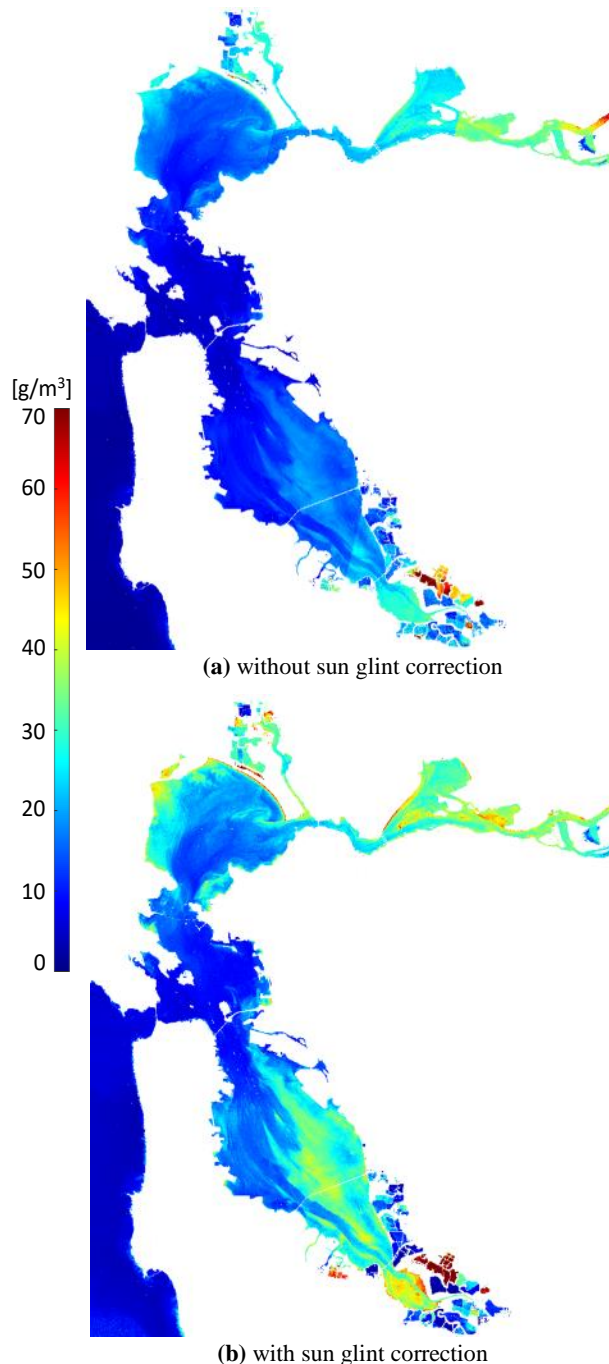


Figure 7. TSM maps derived from OBRA without and with the sun glint correction.

Figure 8 shows the TSM maps derived from the neural network model with and without the glint correction for the same date presented for OBRA. The maps show slight differences indicating the minimal impact of the glint correction on the transferability of the proposed model. The sediment plumes are clear with high TSM concentrations. Visual inspection of the maps (Figures 7 and 8) also indicates the underestimated TSM based on OBRA, which is in line with the matchup statistics (Table 2).

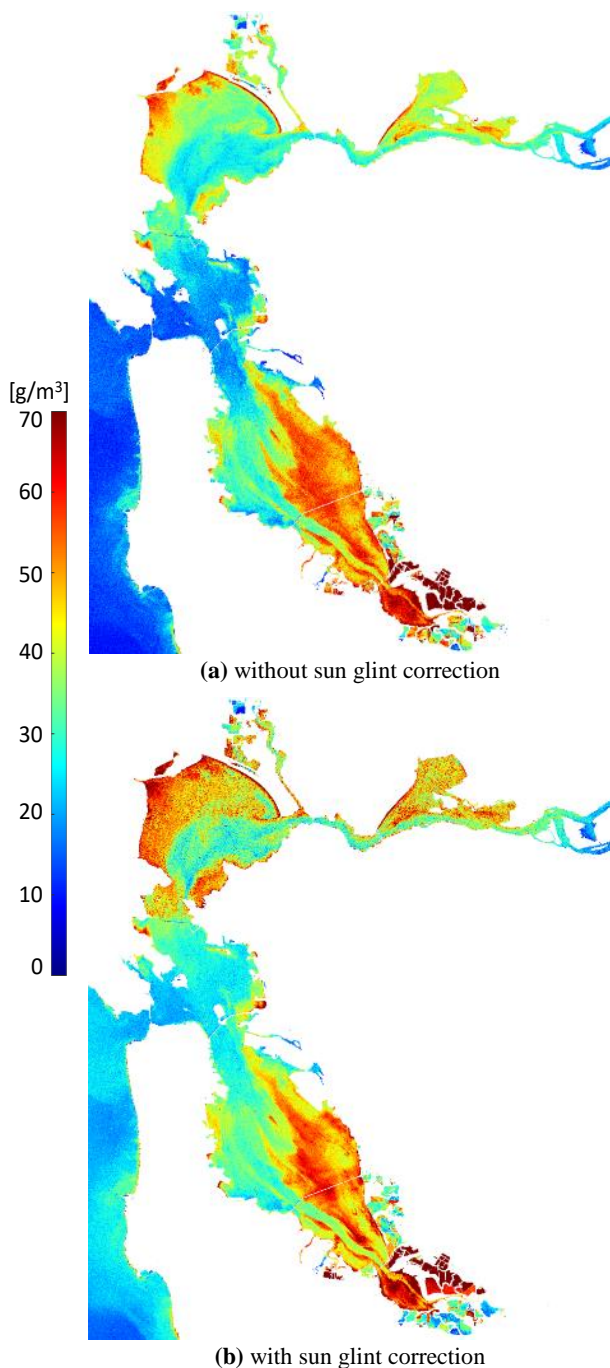


Figure 8. TSM maps derived from NN without and with the sun glint correction.

5. CONCLUSIONS AND OUTLOOKS

This study investigated the temporal transferability of machine learning and band ratio models in retrieving TSM from Sentinel-2 imagery. The results of the ratio model implemented through the OBRA indicated that the optimal bands and performance of the model are not robust when transferring the model to another time than the training period. However, sun glint correction significantly improved the accuracy and robustness of the TSM retrieval. The proposed neural network-based method outperformed the standard OBRA and provided high performance in terms of temporal transferability. The glint correction minimally impacts the results of the proposed model. The better performance and robustness of the proposed method

can be attributed to the capability of the machine learning approach to learn various features from all the spectral bands. This is while the OBRA relies only on a single band ratio feature that can be degraded due to various confounding factors, particularly in the temporal context (e.g., sun glint, atmospheric effects).

The spatial transferability of the TSM retrieval models is an area of investigation for future studies. In this context, more extensive training samples from different water types (e.g., eutrophic, CDOM-rich) would be required to generalize the model. In addition, deep networks would be beneficial to learn high-level and robust features from a huge set of training. Here, we investigated the transferability of models for TSM retrieval. This study can be extended to other constituents (e.g., Chl-a and CDOM). Furthermore, the impact of the spectral resolution of satellite sensors on the transferability of the models also requires investigation. For instance, there is a growing interest in CubeSat imagery for aquatic applications (Niroumand-Jadidi and Bovolo, 2021; Poursanidis et al., 2019). Currently, the spectral resolution of CubeSat data (e.g., PlanetScope imagery) is mainly limited to four bands that may affect the temporal transferability of water quality retrieval models. The robustness of the methods concerning different atmospheric and sun glint correction methods also require further investigation.

REFERENCES

- Bernardo, N., Watanabe, F., Rodrigues, T., Alcântara, E., 2017. Atmospheric correction issues for retrieving total suspended matter concentrations in inland waters using OLI/Landsat-8 image. *Adv. Sp. Res.* 59, 2335–2348.
- Bresciani, M., Pinardi, M., Free, G., Luciani, G., Ghebrehiwot, S., Laanen, M., Peters, S., Della Bella, V., Padula, R., Giardino, C., 2020. The Use of Multisource Optical Sensors to Study Phytoplankton Spatio-Temporal Variation in a Shallow Turbid Lake. *Water* 12, 284.
- Cloern, J.E., Schraga, T.S., Nejad, E., Martin, C., 2020. Nutrient Status of San Francisco Bay and Its Management Implications. *Estuaries and Coasts* 43, 1299–1317.
- Defoin-Platel, M., Chami, M., 2007. How ambiguous is the inverse problem of ocean color in coastal waters? *J. Geophys. Res.* 112, C03004.
- Gege, P., 2004. The water color simulator WASI: An integrating software tool for analysis and simulation of optical in situ spectra. *Comput. Geosci.* 30, 523–532.
- Gholizadeh, M.H., Melesse, A.M., Reddi, L., 2016. A Comprehensive Review on Water Quality Parameters Estimation Using Remote Sensing Techniques. *Sensors* 16.
- Groom, S.B., Sathyendranath, S., Ban, Y., Bernard, S., Brewin, B., Brotas, V., Brockmann, C., Chauhan, P., Choi, J.K., Chuprin, A., Ciavatta, S., Cipollini, P., Donlon, C., Franz, B.A., He, X., Hirata, T., Jackson, T., Kampel, M., Krasemann, H., Lavender, S.J., Pardo-Martinez, S., Melin, F., Platt, T., Santoleri, R., Skakala, J., Schaeffer, B., Smith, M., Steinmetz, F., Valente, A., Wang, M., 2019. Satellite ocean colour: Current status and future perspective. *Front. Mar. Sci.* 6, 485.
- Hansen, C., Burian, S., Dennison, P., Williams, G., 2017. Spatiotemporal Variability of Lake Water Quality in the Context of Remote Sensing Models. *Remote Sens.* 9, 409.

- Jorge, D.S.F., Barbosa, C.C.F., De Carvalho, L.A.S., Affonso, A.G., De, F., Lobo, L., De, E.M.L., Novo, M., Zhang, Y., Giardino, C., Li, L., Mishra, D.R., Thenkabail, P.S., 2017. SNR (Signal-To-Noise Ratio) Impact on Water Constituent Retrieval from Simulated Images of Optically Complex Amazon Lakes. *Remote Sens.* 2017, Vol. 9, Page 644 9, 644.
- Lee, Z., Carder, K.L., Arnone, R.A., 2002. Deriving inherent optical properties from water color: a multiband quasi-analytical algorithm for optically deep waters. *Appl. Opt.* 41, 5755–72.
- Legleiter, C.J., Roberts, D.A., Lawrence, R.L., 2009. Spectrally based remote sensing of river bathymetry. *Earth Surf. Process. Landforms* 34, 1039–1059.
- Ligi, M., Kutser, T., Kallio, K., Attila, J., Koponen, S., Paavel, B., Soomets, T., Reinart, A., 2017. Testing the performance of empirical remote sensing algorithms in the Baltic Sea waters with modelled and in situ reflectance data. *Oceanologia* 59, 57–68.
- Mobley, C.D., 1994. *Light and water: radiative transfer in natural waters.* Academic Press.
- Niroumand-Jadidi, M., Bovolo, F., 2021. Water Quality Retrieval and Algal Bloom Detection Using High-Resolution Cubesat Imagery. *ISPRS Ann. Photogramm. Remote Sens. Spat. Inf. Sci.* V-3–2021, 191–195.
- Niroumand-Jadidi, M., Bovolo, F., Bruzzone, L., 2019. Novel Spectra-Derived Features for Empirical Retrieval of Water Quality Parameters: Demonstrations for OLI, MSI, and OLCI Sensors. *IEEE Trans. Geosci. Remote Sens.* 57, 10285–10300.
- Niroumand-Jadidi, M., Bovolo, F., Bruzzone, L., 2020a. SMART-SDB: Sample-specific multiple band ratio technique for satellite-derived bathymetry. *Remote Sens. Environ.* 251, 112091.
- Niroumand-Jadidi, M., Bovolo, F., Bruzzone, L., 2020b. Water Quality Retrieval from PRISMA Hyperspectral Images: First Experience in a Turbid Lake and Comparison with Sentinel-2. *Remote Sens.* 12, 3984.
- Niroumand-Jadidi, M., Bovolo, F., Bruzzone, L., Gege, P., 2020c. Physics-based Bathymetry and Water Quality Retrieval Using PlanetScope Imagery: Impacts of 2020 COVID-19 Lockdown and 2019 Extreme Flood in the Venice Lagoon. *Remote Sens.* 2020, Vol. 12, Page 2381 12, 2381.
- Niroumand-Jadidi, M., Bovolo, F., Bruzzone, L., Gege, P., 2021. Inter-Comparison of Methods for Chlorophyll-a Retrieval: Sentinel-2 Time-Series Analysis in Italian Lakes. *Remote Sens.* 13, 2381.
- Niroumand-Jadidi, M., Vitti, A., 2016. Optimal band ratio analysis of WorldView-3 imagery for bathymetry of shallow rivers (case study: Sarca River, Italy). In: *International Archives of the Photogrammetry, Remote Sensing and Spatial Information Sciences - ISPRS Archives.*
- Niroumand-Jadidi, M., Vitti, A., Lyzenga, D.R., 2018. Multiple Optimal Depth Predictors Analysis (MODPA) for river bathymetry: Findings from spectroradiometry, simulations, and satellite imagery. *Remote Sens. Environ.* 218, 132–147.
- Overstreet, B.T., Legleiter, C.J., 2017. Removing sun glint from optical remote sensing images of shallow rivers. *Earth Surf. Process. Landforms* 42, 318–333.
- Pitarch, J., Vanhellemont, Q., 2021. The QAA-RGB: A universal three-band absorption and backscattering retrieval algorithm for high resolution satellite sensors. Development and implementation in ACOLITE. *Remote Sens. Environ.* 265, 112667.
- Politi, E., Cutler, M.E.J., Rowan, J.S., 2015. Evaluating the spatial transferability and temporal repeatability of remote-sensing-based lake water quality retrieval algorithms at the European scale: a meta-analysis approach. *Int. J. Remote Sens.* 36, 2995–3023.
- Poursanidis, D., Traganos, D., Chrysoulakis, N., Reinartz, P., 2019. Cubesats Allow High Spatiotemporal Estimates of Satellite-Derived Bathymetry. *Remote Sens.* 11, 1299.
- Ritchie, J.C., Zimba, P. V., Everitt, J.H., 2003. *Remote Sensing Techniques to Assess Water Quality.* Photogramm. Eng. Remote Sens. 69, 695–704.
- Sagan, V., Peterson, K.T., Maimaitijiang, M., Sidike, P., Sloan, J., Greeing, B.A., Maalouf, S., Adams, C., 2020. Monitoring inland water quality using remote sensing: potential and limitations of spectral indices, bio-optical simulations, machine learning, and cloud computing. *Earth-Science Rev.* 205, 103187.
- Schraga, T.S., Cloern, J.E., 2017. Water quality measurements in San Francisco Bay by the U.S. Geological Survey, 1969–2015. *Sci. Data* 2017 41 4, 1–14.
- Seegers, B.N., Stumpf, R.P., Schaeffer, B.A., Loftin, K.A., Werdell, P.J., 2018. Performance metrics for the assessment of satellite data products: an ocean color case study. *Opt. Express* 26, 7404.
- Soomets, T., Uudeberg, K., Jakovels, D., Brauns, A., Zagars, M., Kutser, T., 2020. Validation and comparison of water quality products in baltic lakes using sentinel-2 msi and sentinel-3 OLCI data. *Sensors (Switzerland)* 20.
- Toming, K., Kutser, T., Laas, A., Sepp, M., Paavel, B., Nöges, T., 2016. First Experiences in Mapping Lake Water Quality Parameters with Sentinel-2 MSI Imagery. *Remote Sens.* 8.
- Vandermeulen, R.A., Mannino, A., Craig, S.E., Werdell, P.J., 2020. 150 shades of green: Using the full spectrum of remote sensing reflectance to elucidate color shifts in the ocean. *Remote Sens. Environ.* 247, 111900.
- Vanhellemont, Q., 2019. Adaptation of the dark spectrum fitting atmospheric correction for aquatic applications of the Landsat and Sentinel-2 archives. *Remote Sens. Environ.* 225, 175–192.
- Vanhellemont, Q., Ruddick, K., 2015. Advantages of high quality SWIR bands for ocean colour processing: Examples from Landsat-8. *Remote Sens. Environ.* 161, 89–106.